Available online at www.sciencedirect.com
ScienceDirect
International Journal of Thermal Sciences 47 (2008) 648–658
International Journal of Thermal Sciences
www.elsevier.com/locate/ijts

Investigation on the choking flow characteristics in electronic expansion valves

Jinghui Liu *, Jiangping Chen, Zhijiu Chen

School of Mechanical Engineering, Shanghai, Jiaotong University, Shanghai 2000240, China

Received 7 August 2006; received in revised form 7 May 2007; accepted 9 May 2007

Available online 22 June 2007

Abstract

A one-dimensional model, in which the evaporation wave theory is employed, is developed to investigate the choking flow characteristics in Electronic Expansion Valves (EEV). The results predicted by the model are validated by the experimental data presented by Zhang. The results show that the choking mass flow rate of EEVs calculated by the model, with R22 as working fluid, agrees well with the tested data. The relative deviation between the predictions and Zhang's tested data is in the range from −5% to 6%. Compared with the tested data, the choking mass flow rate of EEVs with the mixture R407c is over-predicted by the model. The pressure at the EEV exit under which choking just occurs is decreased as the flow area is decreased. The trend is consistent with Zhang's experimental results.

Keywords: Choking flow; Electronic Expansion Valve (EEV); Evaporation wave; Refrigeration; Two-phase flow

1. Introduction

An expansion device is one of the four most important parts in refrigeration systems. It is used not only to drop the pressure of the refrigerant to satisfy the need of refrigeration, but also to regulate the mass flow rate of the refrigerant to match the variable load. High responding speed and precision of expansion devices can improve the control quality of refrigeration systems. Thermal expansion valves (TEVs) have been widely used as expansion devices in refrigeration systems. Owing to the slow responding speed and the low precision of TEVs, EEVs were developed in 1980s. Compared with TEVs, EEVs respond faster to the variable load and have wider regulating range and higher precision. They have a promising future to be used in refrigeration systems.

The mass flow rate characteristic for single phase incompressible fluids is usually expressed in the form of Bernoulli equation

$$m = C_d A\sqrt{2\rho_i(P_i - P_o)} \tag{1}$$

where, m is the mass flow rate. A is the flow area. ρ_i is the density of the working fluid at the entrance. P_i and P_o are the pressures at the entrance and the exit respectively. C_d is the mass flow rate coefficient which is a constant for incompressible single phase fluids.

The mass flow rate is a very important parameter of expansion devices. Although phase transition occurs when refrigerant flows through EEVs, Eq. (1) is still usually used to depict the mass flow rate characteristic. From Eq. (1), the mass flow rate seems to be increased with the decreasing pressure at the EEV exit. But in fact, when the pressure at the EEV exit is low enough, the mass flow rate has nothing to do with it. Fig. 1 shows the mass flow rate of an EEV presented by Zhang [1], with R22 and R407c as working fluids, varying with the EEV exit pressure and the number of opening pulses for step motor (flow area). In Fig. 1, the mass flow rate of the EEV is changed little with the pressure at the EEV exit when the pressure at the EEV exit is low enough. Therefore, in order to match the feature, C_d of EEVs must be no longer a constant and should be determined by experiments. In 1935, D.D. Wile [2] first suggested an equation of C_d for TEVs which correlates the inlet density and the exit specific volume of the refrigerant. On the basis of experiments, Ma [3], and Zhang [4] sug-

* Corresponding author. Tel.: +086 02134206585; fax: +086 02134202814.
E-mail address: liujinghui@sjtu.edu.cn (J. Liu).

1290-0729/$ – see front matter
doi:10.1016/j.ijthermalsci.2007.05.006

Nomenclature

A	flow area	m^2
C_d	mass flow rate coefficient	
F_i	flashing index	
J	mass flux	kg/m^2s
h	enthalpy	kJ/kg
k	Boltzmann constant	
m	mass flow rate	kg/s
n	index, pulse number	
P	pressure	Pa
ΔP	pressure difference	Pa
ΔP_{Fi}	pressure undershoot at flashing inception	Pa
R	radius	m
T	temperature	K
T_r	reduced initial temperature	
T_c	critical temperature	K
u	velocity	m/s
x	quality	
σ	surface intension	N/m
υ	specific volume	m^3/kg
ρ	density	kg/m^3
Σ	depressurization rate	Matm/s
Δt_{sc}	subcooled degree	K
Δt_{sh}	superheat degree	K
z	distance	m

Subscripts

f	liquid
g	vapor
s	saturated
i	inlet
o	outlet
t	throat
c	critical
d	diffuser
oc	outlet when choking just occurs

gested two more accurate equations of the C_d and found it is related to the refrigerant states at the entrance and the exit of EEVs and the EEV geometry parameters. The reason that C_d is related to the refrigerant state at the EEVs exit is resulted by the form of Eq. (1). From Fig. 1, it can be deduced that choking must occur when the pressure at the EEV exit is low enough. Now that the choking mass flow rate has nothing to do with the pressure at the EEV exit, equations which depict the choking mass flow rate should not include it. Therefore, Eq. (1) has limitation to depict the choking flow characteristics of EEVs.

From Bernoulli equation, the mass flow rate is influenced by two variables which are the flow area and the pressure difference between the entrance and the exit of the EEVs. Because the sound speed of low quality two-phase fluid is very low (10^0-10^1 m/s), choking usually occurs in EEVs under the running conditions of refrigeration systems. If choking occurs, the mass flow rate is influenced only by the flow area. From the point of view of control, refrigeration systems are easier to level off for one free variable than two free variables. Therefore, choking can improve the control quality of refrigeration systems.

The contributions of P. Reinke and G. Yadigaroglu [5], J.R. Simoes-Moreira [6–9], M.D. Alamgir and J.H. Lienhard [10], V.E. Schrock [11], O.C. Jones Jr. [12], N. Abuaf [13], A.A. Kornahauser [14], G.S. Harrell [15], K. Akagawa et al. [16], M.M. Vieira and J.R. Simoes-Moreira [17] show that rapid depressurization makes the initial subcooled or saturated liquid superheated or metastable. Then the superheated liquid will explosively evaporate in a very narrow and observable region, i.e. evaporation wave. Documentaries [6,7,9, 17] of the evaporation of liquid jet discharging into a low pressure environment using short-duration photographic techniques have revealed that the liquid core in the flashing process takes the shape of a cone. M.M. Vieira and J.R. Simoes-Moreira [17] experimentally investigated the flashing jet with schlieren method and found downstream of the evaporation discontinuity, the two phase flow reaches supersonic and is terminated through a shock wave. The refrigerant's thermodynamic behaviors are very complex in EEVs when choking occurs. Owing to the rapid depressurization when refrigerant flows through EEVs, the liquid refrigerant becomes superheated at a location in EEVs. Then explosive evaporation occurs with sudden pressure drop. J.R. Simoes-Moreira [6,8, 9] developed the evaporation wave theory to investigate the explosive evaporation phenomenon. Assuming refrigerant expansion devices as a convergent nozzle and the refrigerant flashing process as a normal evaporation wave, he investigated pressure drop and flashing mechanism in refrigeration expansion devices [7]. He calculated the refrigerant state immediately downstream the evaporation wave for the given upstream metastable conditions, but did not suggest how to determine the mass flow rate and the refrigerant state just upstream the evaporation wave for a given stagnation condition at the EEV entrance.

Determination of the choking mass flow rate and the refrigerant state immediately upstream the evaporation waves is the key for studying the choking flow characteristics of EEVs. In this paper, N. Abuaf's [13] model for two-phase flow convergent–divergent nozzle is employed to predict the choking mass flow rate and the refrigerant's metastable state immediately upstream the evaporation wave, and Wadle's [18] abrupt diffuser model is employed to predict the pressure recovery downstream the shock wave. Together with the evaporation wave theory, the choking flow characteristics of EEVs are investigated.

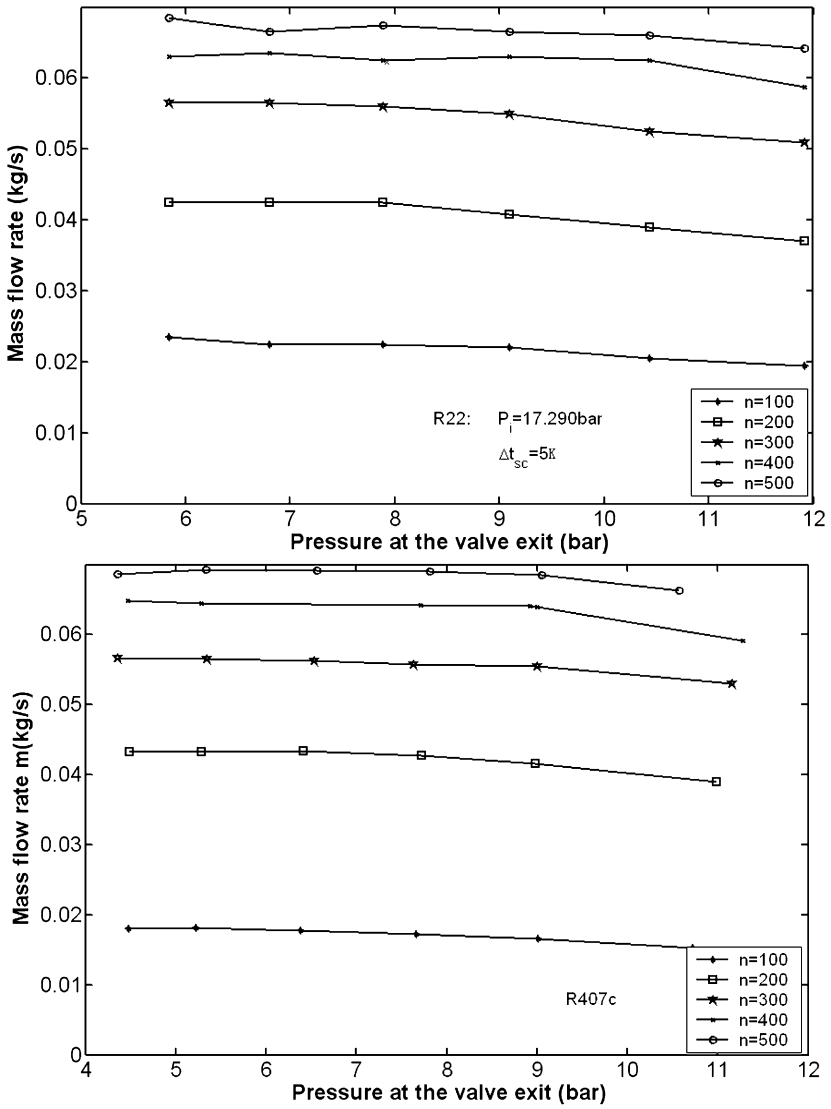

Fig. 1. Data of mass flow rate tested by Zhang [1] varying with the pressure at the EEV exit and the flow area (the number of opening pulses for step motor).

2. The flow passage in EEVs and refrigerant behaviors

2.1. The flow passage in EEVs

The left in Fig. 2 is the structure of the flow passage in EEVs. Shown as in Fig. 2, along the flow direction, the flow area gradually becomes smaller first, and then gradually gets larger. At the exit of the EEV seat hole, the flow area gets larger abruptly. The shape of the flow passage is very like the combination of a convergent–divergent nozzle and an abrupt diffuser, shown as the right in Fig. 2. Since the flow area in EEVs can be adjusted by lifting up or falling down the needle with a step motor, the throat area of the convergent–divergent nozzle is also assumed changeable, just as shown with the dashed-line in Fig. 2.

2.2. Refrigerant behaviors

In order to simplify the problems, some hypotheses are made as the following.

- The inlet velocity, the outlet velocity, friction and heat transfer are neglected.
- The inlet refrigerant is subcooled or saturated liquid.
- The flow is stable. According to Abuaf's [13] results, flashing inception point is located at the minimal area plane (throat).
- The refrigerant immediately downstream the evaporation wave is in homogenous and thermal equilibrium.
- In order to solve the problem with a one-dimensional model, the flashing process is regarded as a normal evaporation wave, just as J.R. Simoes-Moreira [9] did. The equivalent location of the evaporation wave is determined by its equivalent area. The evaporation wave surface is approximated by a hemisphere if it occurs out of the nozzle. J.R. Simoes-Moreira [9] defined the equivalent radius of the hemisphere of the evaporation wave

$$R_h = \sqrt{m \cdot \upsilon_2 / 2\pi u_2} \tag{2}$$

where m is the mass flow rate, υ_2 is the downstream specific volume, and u_2 is the downstream velocity.

The evaporation wave may also occur in the divergent-section of the nozzle. It is approximated by a plane if it occurs in the divergent section of the nozzle.

Shown as in Fig. 3, according to the above hypotheses, along the flow direction, the refrigerant's thermodynamic behaviors are depicted as the following. The subcooled or saturated liquid is increased in velocity and decreased in pressure in the convergent section of the nozzle. Owing to the rapid depressurization, flashing is delayed and at the throat, refrigerant becomes superheated (state 1). Then flashing begins at the throat. At a location in or out of the divergent section, sudden phase transition occurs through an evaporation wave with sudden pressure drop. The velocity of the two-phase flow (state 2) immediately downstream the evaporation wave is sonic in relation to the evaporation wave. If the pressure at the EEV exit is very low, the two-phase refrigerant flow is accelerated to supersonic (2 → 3). Then, the supersonic two-phase flow undergoes a shock wave (3 → 4) to become subsonic at a location downstream the evaporation wave, going with an abrupt pressure rise. The two-phase flow downstream the shock wave is diffused in the abrupt diffuser to match the pressure at the EEV exit.

A shock wave makes the available energy lost, which distinctively affects the pressure recovery in the diffuser. Its location and intensity are determined by the pressure at the EEV exit. As the pressure at the EEV exit is increased, the shock wave approaches to the evaporation wave, and its intensity gets weaker and weaker. When the location of the shock wave is just overlapped with that of the evaporation wave, the state immediately upstream the shock wave is the state immediately downstream the evaporation wave, at which the velocity is just sonic. The shock wave disappears under this condition. The refrigerant immediately downstream the evaporation wave would

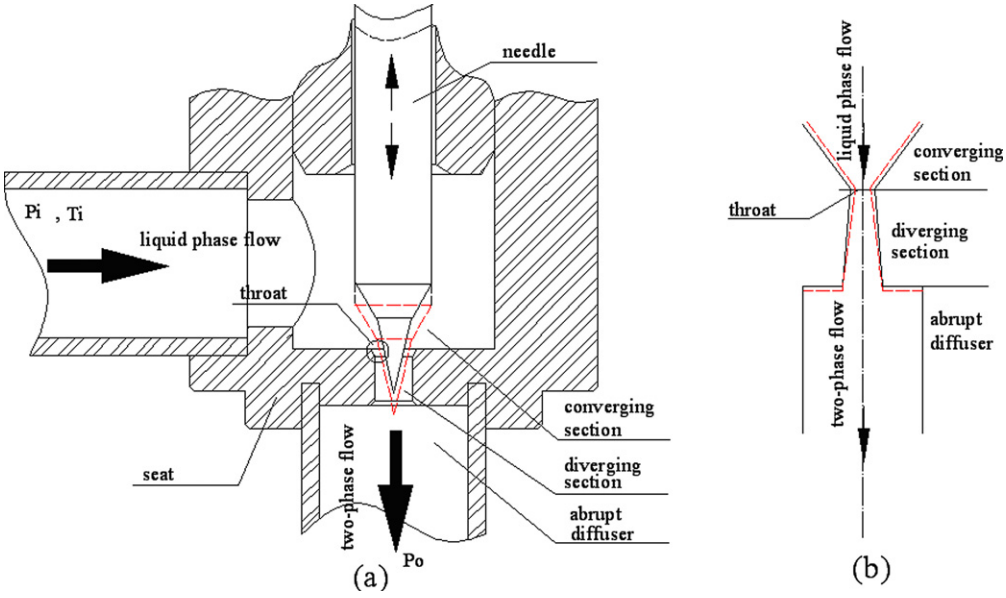

Fig. 2. Diagram of simplification of the flow passage in EEVs.

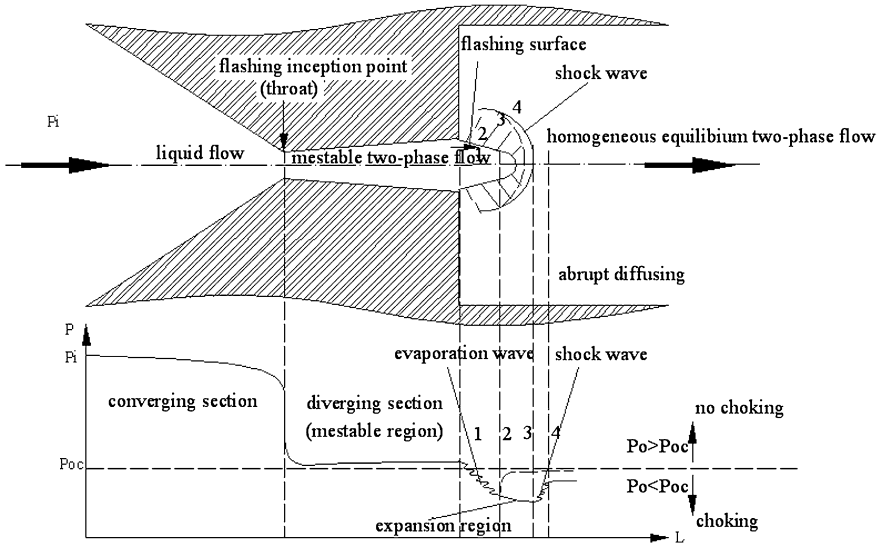

Fig. 3. Diagram of the refrigerant's thermodynamic behavior of choking flow in an EEV.

not be accelerated supersonic, and is diffused immediately in the abrupt diffuser after undergoing the evaporation wave. The corresponding back pressure P_{oc} is the maximal back pressure for choking occurrence. If the pressure at the EEV exit is higher than P_{oc}, no choking occurs.

3. Choking flow characteristics in EEVs

3.1. Choking mass flow rate

Superheated liquid in rapid depressurizing flashing flow has been founds by many investigators [11–15]. Owing to the effect of the metastable state phenomenon, it has been generally found that models based on assumptions of homogeneous equilibrium under-predict the critical discharge rate. Among the models [10, 12,13] which calculate the flashing critical mass flux in nozzles, N. Abuaf's [13] model gives the satisfied accuracy. In this model, the pressure undershoot at the flashing inception location can be calculated by the following equation

$$\Delta P_{Fi}^{*} = \frac{\Delta P_{Fi}}{\Delta P_{Fio}} = \mathrm{Max}\begin{cases} 0 \\ 1 - 27[\frac{\tilde{u}'^2}{u_i^2}][\frac{A}{A_i}]^n F_i \end{cases} \tag{3a}$$

where

$$n = \begin{cases} 1.75, & A/A_i \geqslant 1:6 \\ 1.4, & A/A_i < 1:6 \end{cases} \tag{3b}$$

where ΔP_{Fi} is the pressure difference between the saturated pressure (P_s) corresponding to the inlet temperature and the pressure (P_{Fi}) at the flashing inception location, A and A_i are the areas at the flashing inception location and at the nozzle inlet, the flashing index is defined as $F_i = \rho_f u^2/2\Delta P_{Fio}$, ρ_f is the liquid density, u is the velocity at the flashing inception location, the turbulent intensity $\sqrt{u'^2}/u_i$ can be assumed to be 0.072.

The pressure difference (ΔP_{Fio}) resulted by the static decompression effects can be calculated by Alamgir and Lienhard's [10] semi-empirical equation

$$\Delta P_{Fio} = 0.253\frac{\sigma^{1.5}}{\sqrt{kT_c}}\frac{T_r^{13.73}\sqrt{1+14\Sigma^{0.8}}}{(1-\frac{\upsilon_f}{\upsilon_g})} \tag{4}$$

where T_r is the reduced initial temperature, T_c is the critical temperature, σ is the liquid surface tension, υ_f and υ_g are specific volume of the liquid and the vapor, respectively. k is the Boltzmann constant. Σ is the decompression rate which is defined as

$$\Sigma = \left.\frac{\partial P}{\partial t}\right|_z + u\left.\frac{\partial P}{\partial z}\right|_t \tag{5}$$

The first term on the right-hand side represents the static depressurization rate while the second term represents the additional convective depressurization rate. In the case of stable flow, the additional convective depressurization rate is regarded zero. Abuaf [13] suggested that Σ can be calculated by

$$\Sigma = \frac{J_c^3}{\rho_f^2}\cdot\frac{\mathrm{d}[\ln(A)]}{\mathrm{d}z} \tag{6}$$

where J_c is the choking mass flux, z is the distance along the axial direction.

Abuaf [13] proved that the flashing inception is located at the throat. The refrigerant between the entrance and the throat is liquid. The mass flux can be calculated by Bernoulli equation

$$J_c = C_D\sqrt{2\rho_f(P_i - P_s + \Delta P_{Fi})} \tag{7}$$

Abuaf [13] found that the mass flow rate coefficient C_D are scattered near a value of 0.94 ± 0.04, quite close to the expected single-phase fluid value. The mass flux calculated by the above model is only related to the inlet conditions, and has nothing to do with the back pressure of the nozzle. It can be calculated by solving Eqs. (3)–(7) with an iteration method. The superheated degree and the pressure at the throat can be calculated by

$$\Delta t_{sh} = T_i - T_{ts} \tag{8}$$

$$P_t = P_s - \Delta P_{Fi} \tag{9}$$

3.2. Evaporation wave

After the calculation of the choking mass flow rate and the metastable state by the above model, the state immediately downstream the evaporation wave can be obtained. According to the evaporation wave theory of J.R. Simoes-Moreira [6–9], the evaporation wave is a discontinuity process. In this process, the conservations of mass, momentum, and energy can be written by

$$[J] = [u/\upsilon] = 0 \tag{10}$$

$$[P + uJ] = 0 \tag{11}$$

$$\left[h + u^2/2\right] = 0 \tag{12}$$

where $[f] = f_2 - f_1$.

By combining Eqs. (10) and (11), one can obtain the Rayleigh equation

$$J^2 = -\frac{[P]}{[\upsilon]} \tag{13}$$

The mathematical statement of the maximum mass flow rate is given by $\mathrm{d}J^2 = 0$, which results in

$$\frac{\mathrm{d}\upsilon_2}{\mathrm{d}T_2} = -\frac{1}{J_c^2}\frac{\mathrm{d}p_2}{\mathrm{d}T_2} \tag{14}$$

Solving Eqs. (10) to (14), the state downstream the evaporation wave can be obtained. The solution method is detailedly stated by J.R. Simoes-Moreira [6].

The evaporation wave problem can also be solved by graphical method in a $P-\upsilon$ diagram. The Rayleigh equation (13) can be rewritten by

$$P = -J^2\upsilon + P_1 + J^2\upsilon_1 \tag{15}$$

Combining Eqs. (10)–(12), one can obtain another equation—Rankine–Hugoniot equation

$$[h] = \frac{\upsilon_1 + \upsilon_2}{2}[P] \tag{16}$$

The Rankine–Hugoniot equation can be rewritten by

$$P = \frac{2(h - h_1)}{\upsilon_1 + \upsilon} + P_1 \tag{17}$$

From Eq. (15), one can see that the Rayleigh equation is a group of straight lines varying with the square of the mass flux J^2 in the $P-\upsilon$ diagram. From Eq. (17), one can see that Rankine–Hugoniot equation is a hyperbola in the $P-\upsilon$ diagram. Shown as in Fig. 4, varying with the mass flux J, Eqs. (15) and (17) may have zero, one or two intersection points. When the two curves only have one intersection point which is called the Chapman–Jouguet (C–J) solution, the corresponding mass flux is the choking mass flux.

3.3. Pressure recovery in the abrupt diffuser

If the pressure at the EEV exit is low enough, the refrigerant downstream the evaporation wave will further expand and be terminated by a shock wave. The refrigerant downstream the shock wave will be diffused in the abrupt diffuser. Wadle [18] investigated the pressure recovery for two-phase flow in an abrupt diffuser, and suggested a formula to calculate it.

$$\Delta P_{d\_i} = \left(1-\varepsilon^2\right)\frac{1}{2}m^2K\left[\frac{x_i^2}{\rho_{ig}}+\frac{(1-x_i)^2}{\rho_{if}}\right] \tag{18}$$

where $\varepsilon = A_{id}/A_{od}$ is the area ratio between the inlet and the outlet of the diffuser, K is a constant which is recommended 2/3 by Wadle [18].

As stated in Section 2.2, the maximal back pressure for choking occurrence p_{oc} can be obtained by

$$P_{oc} = P_2 + \Delta P_{d\_2} \tag{19}$$

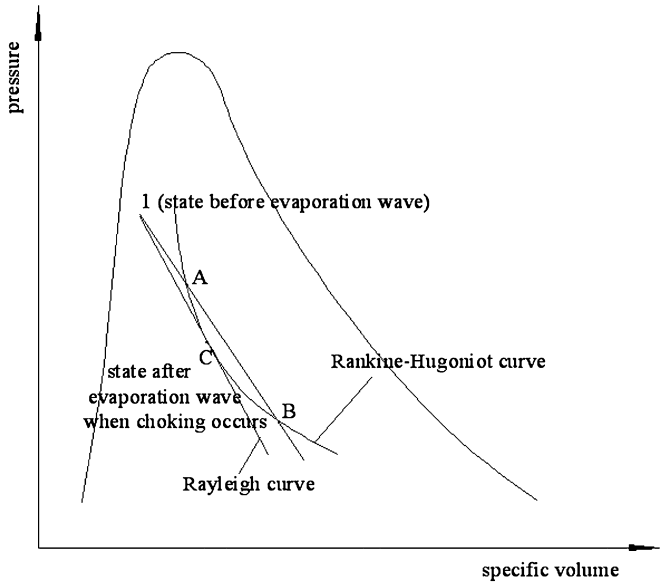

Fig. 4. Graphic solution of evaporation wave in the $P-\upsilon$ diagram.

3.4. Zhang's experiments

In Zhang's experiments, a new thermal cycle system which is called liquid cycle is adopted (Fig. 5). In the rig, the compressor of the refrigeration cycle is replaced to raise the refrigerant pressure by a magnetic pump. A cold bath is installed to subcool the refrigerant after its flashing in the EEV. The high pressure subcooled refrigerant is heated by the hot bath to the same inlet condition as that in a refrigeration system. The magnetic pump is used to control the inlet pressure; the high pressure heat exchanger I is used to control inlet temperature; and the low pressure heat exchanger II is used to control outlet pressure.

The refrigerants used in Zhang's study are R22 and its alternative refrigerant R407c. The test conditions are listed in Table 1.

The test EEV is driven by a step motor. The diameter of the seat hole is 1.8 mm. Corresponding to the EEV opening degrees of 100, 200, 300, 400 and 500 opening pulses, the flow areas are 0.6310, 1.1697, 1.6162, 1.9705 and 2.2325 mm^2, respectively. The flow area of this type of EEV can be fitted into a parabola curve [1]

$$\begin{cases} A = -0.17z^2 + 1.3\times 10^{-3}z \\ z = n/192\,000 \end{cases} \tag{20}$$

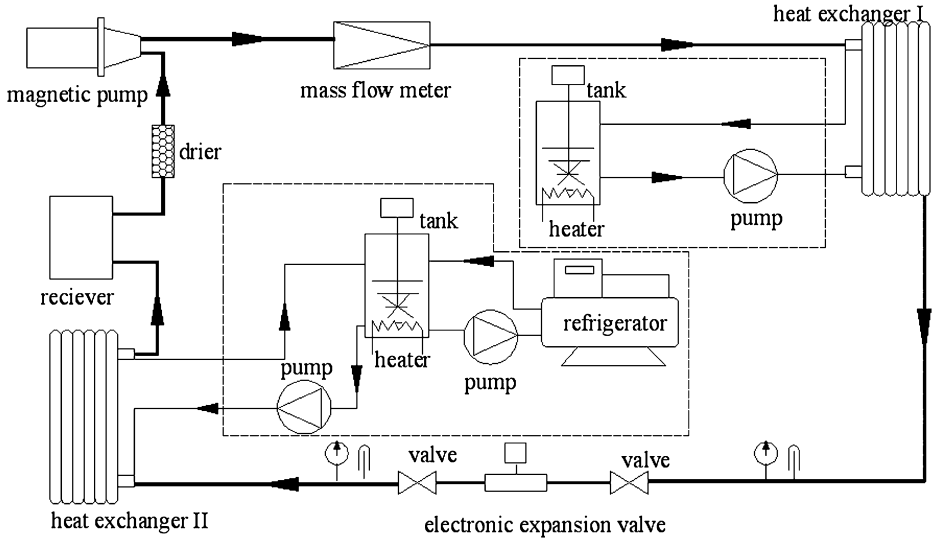

Fig. 5. Schematic of Zhang's test rig.

where, z is the lifting distance of the needle. Then

$$\frac{\mathrm{d}[\ln(A)]}{\mathrm{d}z} = \frac{1.3 \times 10^{-3} - 0.34z}{1.3 \times 10^{-3}z - 0.17z^2} \tag{21}$$

In this paper, the flow area is represented by the number of opening pulses (n) for the step motor.

Table 1
Test conditions of Zhang's experiment

No.		Inlet pressure (bar)	Outlet pressure (bar)	Subcooled degree (K)
1	R22	17.290	5.838, 6.807, 7.891, 9.099, 10.439, 11.919	5
	R407c	16.225	4.359, 5.123, 6.538, 7.629, 8.921, 11.160	4
2	R22	11.919, 13.548, 15.335, 17.290, 19.423	6.807	5
	R407c	10.36, 12.126, 14.123, 16.225, 18.462	5.123	4
3	R22	15.335	6.807	3, 6, 9, 12, 15
	R407c	14.123	5.123	3, 6, 9, 12

4. Result and discussion

4.1. The choking mass flow rate

Fig. 6 shows the comparison of the choking mass flow rate between the calculated data and the experimental data presented by Zhang [1]. The relative deviation between the data calculated by the model and the tested data is shown in Fig. 7. As the flow area and the inlet pressure are increased, the choking mass flow rate is increased. The less the flow area is, the faster the choking mass flow rate is increased. The choking mass flow rate calculated by the model with R22 agrees well with the tested data. The relative deviation of the choking mass flow rate with R22 is ranged from −5% to 6% except when the number of opening pulses is 100 under which the deviation is between 21% and 30%. The reason for this may be that choking does not occur when the opening pulse number is 100, because the pressure at the EEV exit under which choking just occurs for 100 opening pulses is apparently lower than that for the others. The next text will explain the reason. The choking mass flow

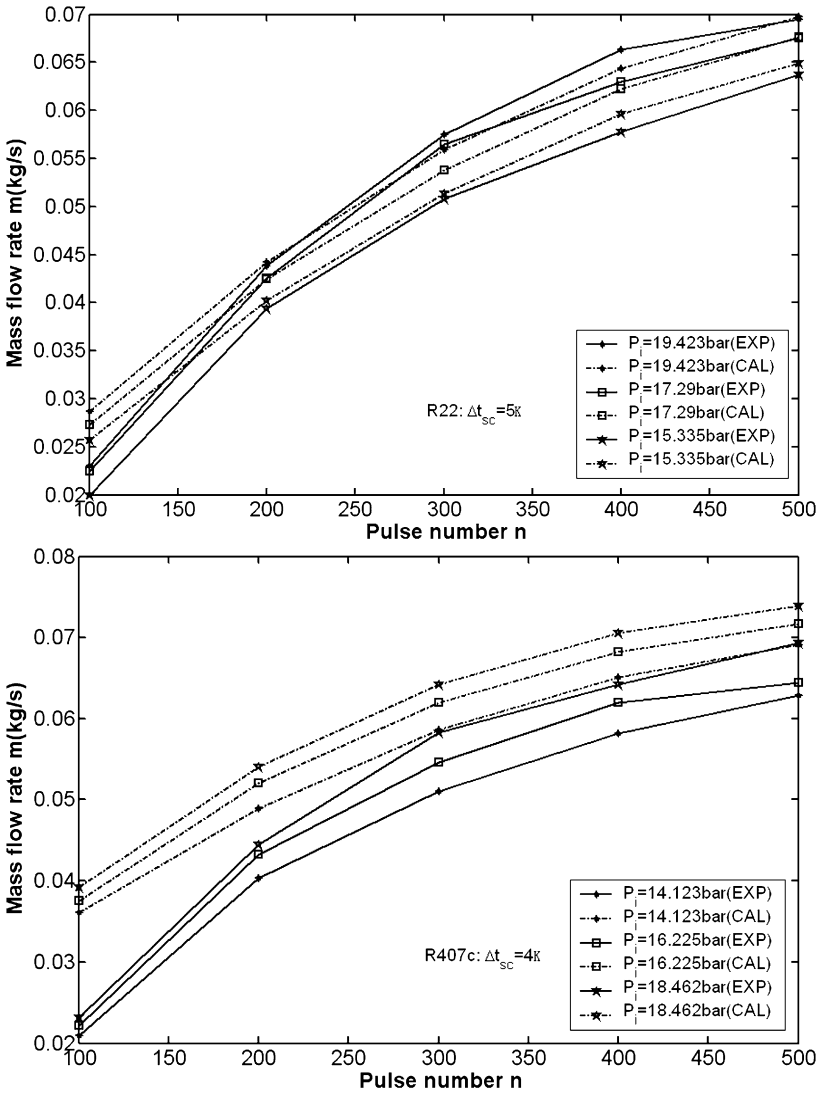

Fig. 6. Comparison of choking mass flow rate between the calculated data and the experimental data.

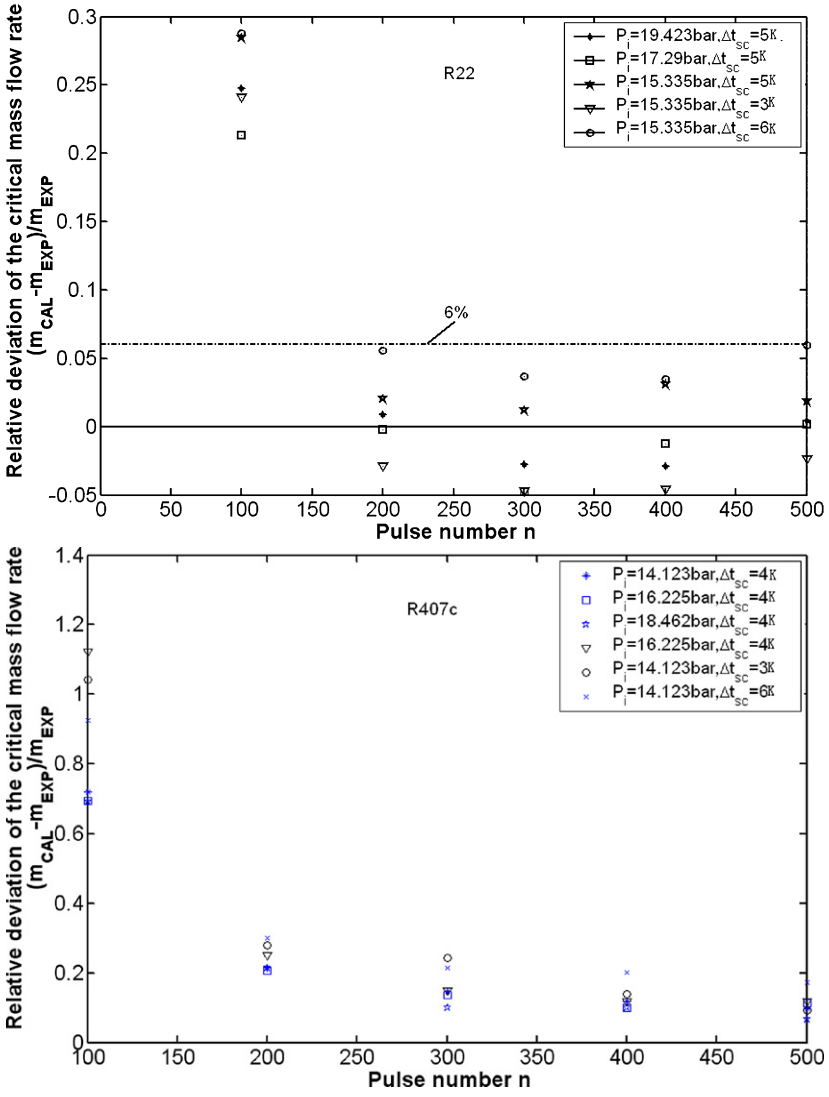

Fig. 7. Comparison of relative deviation of the choking mass flow rate between the calculated data and the experimental data.

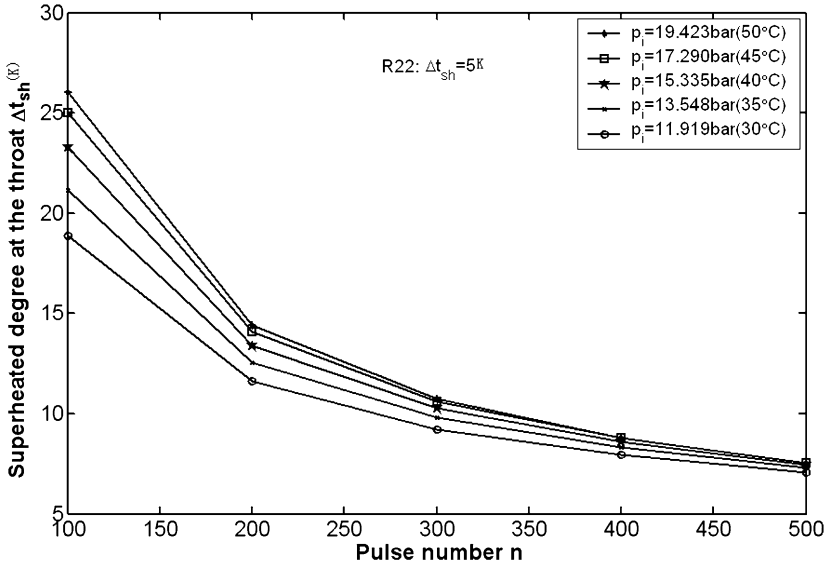

Fig. 8. Superheated degree at the throat varying with the flow area and the inlet pressure.

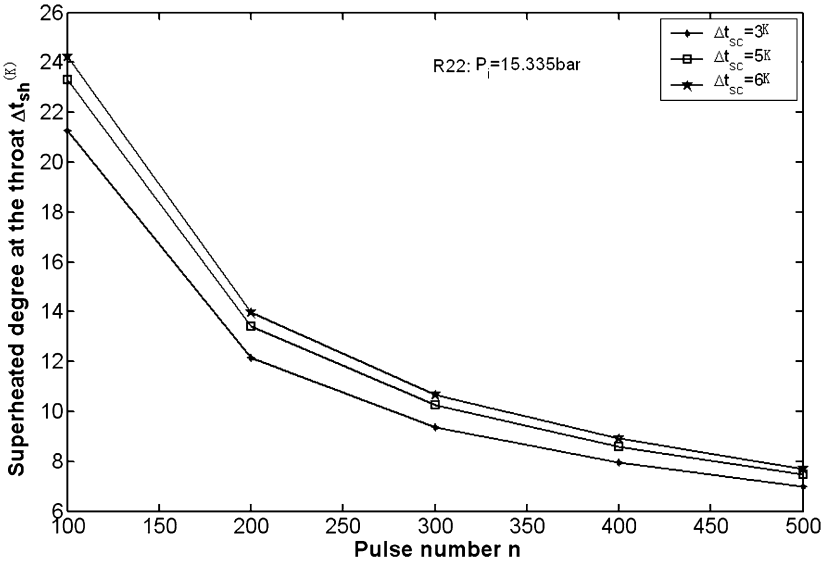

Fig. 9. The superheated degree at the throat varying with the flow area and the inlet subcooled degree.

Table 2
Numerical results of the model solution (R22)

Control parameters	Pulses n	$P_t(P_1)$ bar	Δt_{sh} K	P_2 bar	x_2	υ_2 m^3/kg	u_2 m/s	m_c kg/s	P_{oc} bar
$P_i = 19.43$ bar	100	8.839	26.05	7.069	0.212	0.00771	56.8	0.0287	7.431
$\Delta t_{sc} = 5$ K	200	12.114	14.39	9.686	0.153	0.00443	49.7	0.0442	10.176
	300	13.302	10.74	10.637	0.132	0.00367	47.0	0.0559	11.196
	400	13.965	8.80	11.163	0.122	0.00331	45.5	0.0644	11.770
	500	14.426	7.50	11.538	0.114	0.00307	44.2	0.0698	12.180
$P_i = 17.29$ bar	100	7.884	25.04	6.305	0.198	0.00805	53.8	0.0273	6.599
$\Delta t_{sc} = 5$ K	200	10.706	14.06	8.562	0.143	0.00466	47.2	0.0424	8.962
	300	11.73	10.61	9.384	0.125	0.00386	44.6	0.0538	9.839
	400	12.301	8.78	9.838	0.114	0.00349	43.2	0.0622	10.333
	500	12.698	7.54	10.155	0.107	0.00325	42.1	0.0676	10.68
$P_i = 15.34$ bar	100	7.166	23.29	5.7328	0.182	0.00811	50.4	0.0257	5.976
$\Delta t_{sc} = 5$ K	200	9.510	13.41	7.608	0.133	0.00483	44.5	0.0402	7.935
	300	10.363	10.27	8.290	0.116	0.00404	42.2	0.0514	8.662
	400	10.839	8.60	8.672	0.107	0.00366	40.9	0.0596	9.075
	500	11.171	7.46	8.936	0.101	0.00342	40.0	0.0649	9.364
$P_i = 15.34$ bar	100	8.066	21.25	6.449	0.175	0.00708	49.2	0.0242	6.718
$\Delta t_{sc} = 3$ K	200	10.393	12.16	8.312	0.129	0.00439	43.2	0.0369	8.666
	300	11.196	0.38	8.956	0.114	0.00375	41.0	0.0467	9.351
	400	11.627	7.94	9.302	0.106	0.00344	39.7	0.0539	9.723
	500	11.919	7.00	9.535	0.100	0.00325	38.9	0.0586	9.976
$P_i = 15.34$ bar	100	6.765	24.22	5.411	0.184	0.00866	51.0	0.0264	5.643
$\Delta t_{sc} = 6$ K	200	9.105	13.98	7.283	0.134	0.00506	45.1	0.0417	7.599
	300	9.975	10.68	7.979	0.117	0.00419	42.8	0.0534	8.341
	400	10.467	8.90	8.372	0.108	0.00377	41.5	0.0621	8.766
	500	10.814	7.68	8.650	0.101	0.00350	40.5	0.0678	9.070

rate with R407c is over-predicted by the model. As the number of the opening pulses is decreased, the relative deviation is increased. It nearly reaches 100% when the number of the opening pulses is 100. The reason for this may be that R407c is a mixture which consists of R23 (23%), R125 (25%), and R134a (52%). About 7.3 K temperature glide exists between the bubble point and the dew point. During the expansion process, the component with low boiling point of the mixture may evaporate first, which reduces the metastable degree at the throat. Alamgir and Lienhard's [10] model was developed on the basis of water. It may not be applicable to the non-azeotropic mixture refrigerants. To explain the phenomenon sufficiently, more investigation is needed.

The superheated degree at the throat varying with the flow area, the inlet pressure and the inlet subcooled degree is shown in Figs. 8 and 9. The superheated degree at the throat is increased with the decreasing flow area. The smaller the flow area is, the faster the superheated degree is increased. With the increasing inlet pressure and the increasing inlet subcooled degree, the superheated degree at the throat is increased.

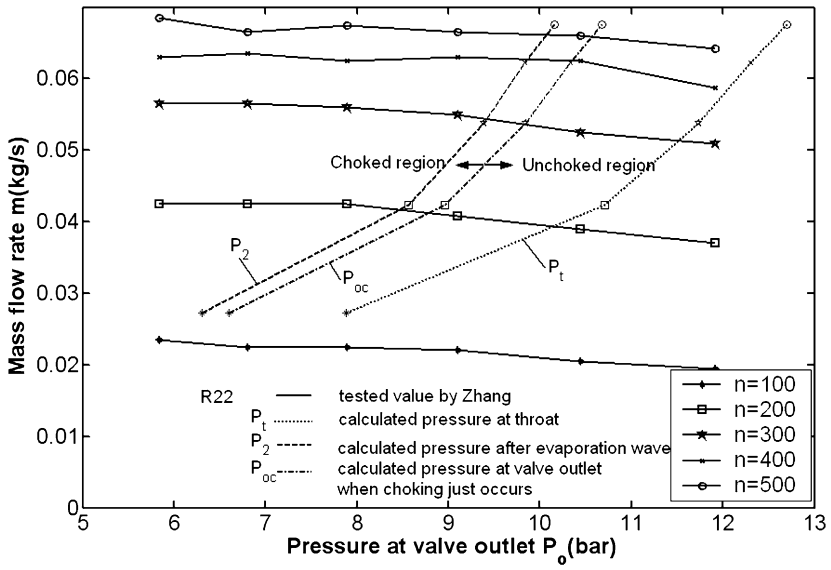

Fig. 10. The tested mass flow rate varying with the flow area and the exit pressure [1], and the pressure at the EEV exit when choking just occurs varying with the flow area calculated by this model.

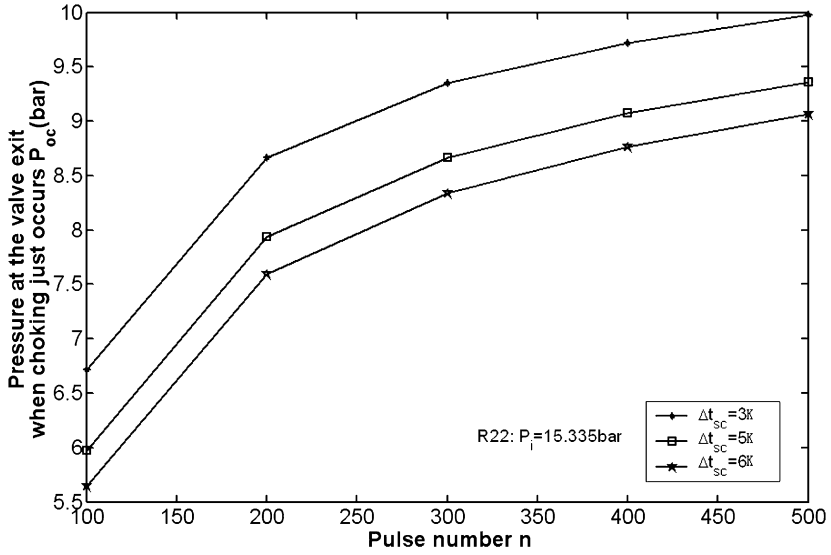

Fig. 11. The pressure at the EEV exit when choking just occurs varying with the flow area and the inlet subcooled degree.

4.2. Choking conditions

How low is the pressure at the EEV exit when choking just occurs? This question can be answered by solving this model. The numerical solution of the model is listed in Table 2.

The pressure at the throat (P_t), the pressure immediately downstream the evaporation wave (P_2), and the pressure at the EEV exit under which choking just occurs (P_{oc}), varying with the opening pulses, are shown in Fig. 10. In order to validate the calculation, the mass flow rate tested by Zhang varying with the pressure at the EEV exit are also presented in the same figure. The abscissa of Fig. 10 represents the pressure at the EEV exit for the tested data, and also indicates the pressure values for the calculated data. The ordinate represents the mass flow rate corresponding to the pressure. From Fig. 10, the pressure at the throat (P_t), the pressure immediately downstream the evaporation wave (P_2), and the pressure at the EEV exit under which choking just occurs (P_{oc}) are all increased as the number of the opening pulses is increased. The less the flow area is, the lower the pressure at the EEV exit under which choking just occurs is. The reason for this is that owing to the relatively higher depressurization rate in the convergent section for the smaller flow area than that for the larger flow area, the metastable degree is increased and the pressure at the throat is decreased as the flow area is decreased. The evaporation wave for the smaller flow area is more intensive than that for the larger flow area. Therefore, the above large deviation of the choking mass flow rate with R22 between the calculated data and the tested data when the opening pulse number is 100 may be resulted by the reason that choking does not occur because the EEV exit pressure is not low enough.

The inlet subcooled degree also affects the pressure at the EEV exit under which choking just occurs. The influence is shown in Fig. 11. From this figure, the pressure at the EEV exit under which choking just occurs is decreased as the inlet subcooled degree is increased. This means that the higher the inlet subcooled degree is, the more difficult choking occurs.

5. Conclusion

A one-dimensional model is developed to investigate the choking flow characteristics in EEVs. Numerical solution is carried out. The data predicted by the model are compared with the experimental data.

The results show that the choking mass flow rate of EEVs calculated by the model, with R22 as working fluid, agrees well with the tested data. The relative deviations between the predictions and Zhang's tested data are in the range from -5% to 6%. Compared with the tested data, the choking mass flow rate of EEVs with the mixture R407c is over-predicted by the model. The relative deviation is larger than that with R22. Owing to the relatively higher depressurization rate in the convergent section for the smaller flow area than that for the larger flow area, the superheated degree of the liquid refrigerant at the throat is increased and the pressure at the throat is decreased, as the throat flow area is decreased. The evaporation wave for the smaller flow area is more intensive than that for the larger flow area. Therefore, the pressure at the EEV exit under which choking just occurs is decreased as the flow area is decreased. The trend is consistent with Zhang's test result.

References

[1] Ch. Zhang, S. Ma, J. Chen, Z. Chen, Experimental analysis of R22 and R407c flow through electronic expansion valve, Energy Conversion and Management 47 (5) (2006) 529–544.

[2] D.D. Wile, The measurement of expansion valve capacity, Refrigeration Engineering 8 (1935) 108–112.

[3] S.W. Ma, Ch. Zhang, J.P. Chen, Z.J. Chen, Experimental study on mass flow rate coefficient of electronic expansion valve, Journal of Shanghai Jiaotong University 39 (2) (2005) 247–250.

[4] Ch. Zhang, Research on characteristics of electronic expansion valve and valve head compensation to middle–small refrigeration systems, Ph.D. dissertation, Shanghai Jiaotong University, 2006.

[5] P. Reinke, G. Yadigaroglu, Explosive vaporization of superheated liquids by boiling front, International Journal of Multiphase Flow 27 (9) (2001) 1487–1516.

[6] J.R. Simoes-Moreira, Oblique evaporation waves, Shock Waves 10 (2000) 229–234.

[7] J.R. Simoes-Moreira, C.W. Bullard, Pressure drop and flashing mechanisms in refrigerant expansion devices, International Journal of Refrigeration 26 (7) (2003) 840–848.

[8] J.R. Simoes-Moreira, J.E. Shepherd, Evaporation waves in superheated dodecane, Journal of Fluid Mechanics 382 (1999) 63–86.

[9] J.R. Simoes-Moreira, M.M. Vieira, E. Angelo, Highly expanded flashing liquid jets, Journal of Thermophysics and Heat Transfer 16 (3) (2002) 415–424.

[10] M.D. Alamgir, J.H. Lienhard, Correlation of pressure undershoot during hot water depressurization, ASME Journal of Heat Transfer 103 (1981) 52–55.

[11] V.E. Schrock, E.S. Starkman, R.A. Brown, Flashing flow of initially subcooled water in convergent–divergent nozzles, ASME Journal of Heat Transfer 99 (1977) 263–268.

[12] O.C. Jones Jr., Flashing inception in flowing liquid, ASME Journal of Heat Transfer 102 (1980) 754–764.

[13] N. Abuaf, O.C. Jones Jr., B.J.C. Wu, Critical flashing flows in nozzles with subcooled inlet conditions, ASME Journal of Heat Transfer 105 (1983) 379–383.

[14] A.A. Kornahauser, P. Menegay, Method of reducing flow metastability in an ejector nozzle, U.S. Patent No. 5,343,711, assigned to Virginia Tech Intellectual Properties, Inc., Blacksburg, VA, 1994.

[15] G.S. Harrell, Testing and modeling of a two-phase ejector, Ph.D. dissertation, Virginia Polytechnic Institute and State University, 1997.

[16] K. Akagawa, T. Fujii, J. Ohta, K. Inoue, K. Taniguchi, Performance characteristics of divergent–convergent nozzles for subcooled hot water, JSME International Journal, Series II 31 (4) (1988) 718–726.

[17] M.M. Vieira, J.R. Simoes-Moreira, Low-pressure flashing mechanisms in iso-octane liquid jet, Journal of Fluid Mechanics 572 (2007) 121–144.

[18] M. Wadle, A new formula for the pressure recovery in an abrupt diffuser, International Journal of Multiphase Flow 15 (2) (1989) 241–256.